

# All-Optical Signal Processing with Semiconductor Optical Amplifiers and Tunable Filters

Xinliang Zhang, Xi Huang, Jianji Dong, Yu Yu, Jing Xu and Dexiu Huang  
*Wuhan National Laboratory for Optoelectronics,  
Huazhong University of Science and Technology  
P.R.China*

## 1. Introduction

All-optical signal processing has been and is receiving more and more attention all over the world because it can increase the capacity of the optical networks greatly in avoiding of the Optical-Electrical-Optical (O/E/O) conversion process, and it can also reduce the system power consumption to a great extent and then increase the system stability. All-optical signal processing can be widely used in optical signal regeneration and switching in next-generation optical networks (Yoo 1996; Danielsen et al. 1998; Saruwatari 2000), such as Optical Time Division Multiplexing (OTDM), Optical Orthogonal Frequency Division Multiplexing (OOFDM), Optical Code Division Multiplexing Accessing (OCDMA), Optical Packet Switching (OPS) and so on. There are many different elemental functions in all-optical signal processing: all-optical wavelength conversion, all-optical logic operation, all-optical 3R regeneration, all-optical format conversion, all-optical sampling, all-optical time demultiplexing, all-optical buffering, etc. It should be mentioned that all-optical wavelength conversion is one of the most important technologies, and it is the basis of other functions. In past two decades, many schemes have been proposed to demonstrate all-optical signal processing functions, and nonlinearities in passive and active waveguides, such as high nonlinear fiber (Olsson et al., 2001), periodic-poled LiNbO<sub>3</sub> (Langrock et al., 2006), silicon-based waveguides (Haché & Bourgeois 2000), chalcogenide-based waveguides (Ta'eed et al., 2006) and semiconductor optical amplifiers (SOAs) (Liu et al., 2006; Stubkjaer 2000), are elemental mechanisms for these schemes. SOA is one of powerful candidates for all-optical signal processing because of its various nonlinear effects, low power consumption, small footprint and possibility to be integrated, therefore, SOAs have been receiving the most widely attention and have been exploited to realize nearly all functions for all-optical signal processing.

In SOAs, nonlinear effects such as cross-gain modulation (XGM), cross-phase modulation (XPM), four-wave mixing and transient cross-phase modulation can all be exploited to demonstrate all-optical signal processing functions (Durhuus et al., 1996; Stubkjaer 2000). Taking all-optical wavelength conversion as an example, XGM wavelength conversion has some advantages such as simple structure, large dynamic optical power range, high conversion efficiency and large operation wavelength range, but it also has some problems

Source: *Advances in Lasers and Electro Optics*, Book edited by: Nelson Costa and Adolfo Cartaxo, ISBN 978-953-307-088-9, pp. 838, April 2010, INTECH, Croatia, downloaded from SCIYO.COM

such as extinction ratio degradation and chirp (Durhuus et al., 1996); XPM wavelength conversion has some characteristics such as good output performance but small dynamic range and difficult to control and fabricate (Durhuus et al., 1996); FWM wavelength conversion (Kelly et al., 1998) is bitrate and format transparent but low conversion efficiency and narrow operation wavelength range; transient XPM conversion is inherent high operation speed but low conversion efficiency.

While used in all-optical signal processing, the input probe signals of SOAs will experience amplitude and phase variations which are induced by carrier density or distribution variations taken by other input pump signals. The optical spectra of the input signals will experience broadening and shifting processes in which the information to be processed is included. Therefore, the SOA can be regarded as spectrum transformer. Combining with appropriate filtering process, all-optical signal processing function can be realized correspondingly. For different filtering processes, we can demonstrate different signal processing functions.

Regarding filtering processes, there are many schemes to realize and demonstrate, such as BPF filters, microring resonators, delay interferometers (fiber-based, silicon waveguide based, LiNbO<sub>3</sub> waveguide based, PMF loop mirror, etc.), FP etalons, dispersive fibers, arrayed waveguide grating (AWG) and so on. Usually we should cascade two or more different kinds of filters to get better output results. It is very important to choose and optimize the filtering processes to realize desired functions and improve the output performance.

In this chapter, we theoretical and experimental analyzed all-optical signal processing with SOAs and tunable filters where SOAs were regarded as spectrum transformers and tunable filters were used to realize different filtering processes and then different signal processing functions. In section 2, complicated theoretical model for SOA is presented, and many nonlinear effects are taken into consideration, such as carrier heating, spectral hole burning, etc. On the other hand, a theoretical model for optimizing the filtering process is also presented. These two theoretical models are value for any different signal processing functions. In section 3, experimental research on all-optical wavelength conversion is discussed and analyzed. In section 4, experimental results for all-optical logic operation are presented. Finally, multi-channel all-optical regenerative format conversion is experimental investigated in section 5. Some remarks are also given in final conclusions.

## 2. Theoretical model

In order to represent the generality for different kinds of signal processing functions, we establish a general theoretical model based on SOA's model and filter's model. As shown in Fig.1, a SOA is cascaded with two basic filters: an optical bandpass filter (OBF) and a delay

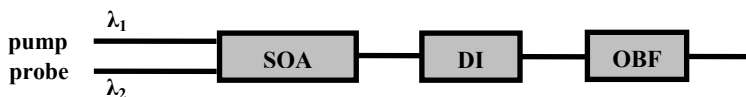


Fig. 1. Schematic diagram for signal processing with SOA and filters

interferometer (DI). These two filters are the most possible to be used to realize signal processing functions. The theoretical model corresponding to Fig. 1 can be exploited to analyze any kinds of signal processing functions. The key point of this model is calculating out the output signal spectrum after the SOA based on a complicated SOA model. Only all kinds of nonlinear effects are taken into account, the accuracy of the output spectrum can be believed. The final output signal spectrum can be analyzed with the help of transmission functions of the cascaded two filters. With iFFT tool, we can get output signal waveform in time domain.

## 2.1 Theoretical model of SOAs

Based on theoretical models in literatures (Mork & Mark 1995; Mork, et al., 1994; Mork & Mark 1992; Agrawal & Olsson 1989; Mork & Mecozzi 1996), we can derive theoretical model for SOAs in which ultrafast nonlinear effects are taken into account. Firstly, the propagation equation for the input signal in the SOA can be derived as the following equation:

$$\frac{\partial A(z, \tau)}{\partial z} = \left[ \frac{1}{2} \Gamma g(z, \tau) - \frac{1}{2} \Gamma_2 \beta_2 (1 + i\alpha_2) |A(z, \tau)|^2 - \frac{1}{2} \Gamma \beta_c n_c(z, \tau) - \frac{1}{2} \Gamma \beta_v n_v(z, \tau) - \frac{1}{2} \alpha_{\text{int}} \right. \\ \left. + \frac{i}{2} [\alpha g_N(z, \tau) + \alpha_{CH} \Delta g_{CH}(z, \tau) + \alpha_{SHB} \Delta g_{SHB}(z, \tau)] \right] A(z, \tau) \quad (1)$$

In Eq.(1), the first to fifth terms on the right hand side represent the linear gain, two-photon absorption (TPA), FCA in conduction band, FCA in valence band and linear absorption loss respectively. The last three terms represent phase modulation process accompanied with linear gain variation, carrier heating and spectral hole burning, which are corresponding to parameters  $\alpha$ ,  $\alpha_{CH}$  and  $\alpha_{SHB}$  respectively.

In order to calculate the gain coefficient, the local carrier densities should be calculated out firstly. The local carrier densities satisfy the following two equations (Mork, et al., 1994):

$$\frac{\partial n_c(z, \tau)}{\partial \tau} = -\frac{n_c(z, \tau) - \bar{n}_c(z, \tau)}{\tau_{1c}} - v_g g(z, \tau) S - n_c(z, \tau) \beta_c v_g S \quad (2)$$

$$\frac{\partial n_v(z, \tau)}{\partial \tau} = -\frac{n_v(z, \tau) - \bar{n}_v(z, \tau)}{\tau_{1v}} - v_g g(z, \tau) S - n_v(z, \tau) \beta_v v_g S \quad (3)$$

The first terms on the right hand sides of Eq. (2) and (3) describe the relaxation process of the electrons and holes to their quasi-equilibrium values  $\bar{n}_c(z, \tau)$  and  $\bar{n}_v(z, \tau)$ , respectively. These relaxation processes are driven by the electron-electron and hole-hole interaction with time constant of  $\tau_{1c}$ ,  $\tau_{1v}$ . The second terms describe carrier consumption due to stimulated emission, and the last terms corresponding to carrier consumption due to two photon absorption.

In this theoretical model, the gain can be expressed as the following equations:

$$\left\{ \begin{aligned} g(z, \tau) &= \frac{1}{v_g} a(\omega_0) [n_c(z, \tau) + n_v(z, \tau) - N_0] \\ g_N(z, \tau) &= \frac{1}{v_g} a(\omega_0) [n_c^*(z, \tau) + n_v^*(z, \tau) - N_0] \\ \Delta g_{CH}(z, \tau) &= \frac{1}{v_g} a(\omega_0) [\bar{n}_c - n_c^*(z, \tau) + \bar{n}_v - n_v^*(z, \tau)] \\ \Delta g_{SHB}(z, \tau) &= \frac{1}{v_g} a(\omega_0) [n_c - \bar{n}_c + n_v - \bar{n}_v] \end{aligned} \right. \tag{4}$$

where  $a(\omega_0)$  is the differential gain coefficient, and  $N_0$  is the transition density of states in optically coupled region.  $g$  is total gain dynamics,  $g_N$  the gain changes accompanied with carrier density variation due to interband recombination,  $\Delta g_{CH}$  the gain changes due to CH,  $\Delta g_{SHB}$  the gain changes due to SHB.

In order to solve Eqs. (2) ~ (4),  $\bar{n}_R(z, \tau)$ ,  $n_R^*(z, \tau)$ ,  $R \in [c, v]$  should be got firstly, and they can be defined as:

$$n_R(z, \tau) = N_0 F(E_{fR}, T_R(z, \tau), E_R) \tag{5}$$

$$n_R^*(z, \tau) = N_0 F(E_{fR}, T_L, E_R) \tag{6}$$

where  $E_{fc}$  and  $E_{fv}$  are the quasi-Fermi level in the conduction band and the valence band, respectively.  $T_C$  and  $T_V$  are the temperature of the carriers in the conduction band and the valence band.  $T_L$  is the lattice temperature.  $E_C$  and  $E_V$  are the corresponding transition energies in the conduction band and the valence band.  $F$  is the Fermi-Dirac distribution function shown as follows:

$$F(\mu, T, E) = \frac{1}{1 + \exp\left(\frac{E - \mu}{k_b T}\right)} \tag{7}$$

To calculate instantaneous carrier temperature ( $T_R$ ) and quasi-Fermi level ( $E_{fR}$ ), we need calculate the total electron-hole pair density  $N$  and the energy state densities  $U$ . The total electron-hole pair density satisfies the following equation:

$$\frac{\partial N(z, \tau)}{\partial \tau} = \frac{I}{eV} - \frac{N}{\tau_s} - v_g g(z, \tau) S + v_g \beta_2 S^2 \tag{8}$$

It should be noted that,  $N(z, \tau)$  counts all the electron-hole pairs, including those that are not directly available for the stimulated emission.

The energy state densities satisfy the following two questions:

$$\frac{\partial U_c(z, \tau)}{\partial \tau} = \beta_c \hbar \omega_0 n_c S - E_c v_g g(z, \tau) S + E_{2c} v_g \beta_2 S^2 - \frac{U_c(z, \tau) - \bar{U}_c(z, \tau)}{\tau_{hc}} \tag{9}$$

$$\frac{\partial U_v(z, \tau)}{\partial \tau} = \beta_v \hbar \omega_0 n_v S - E_v v_g g(z, \tau) S + E_{2v} v_g \beta_2 S^2 - \frac{U_v(z, \tau) - \bar{U}_v(z, \tau)}{\tau_{hv}} \tag{10}$$

In these equations, the first terms describe the change in energy density due to the stimulated emission. The second terms depict the changes due to FCA and the third terms account for the TPA. The last terms represent the relaxation to equilibrium due to carrier-phonon interactions with time constant of  $\tau_{hc}$  and  $\tau_{hv}$ . The equilibrium energy densities are defined as:

$$\bar{U}_c = \frac{1}{V} \sum_k \frac{\hbar k^2}{2m_c^*} F(E_{fc}(z, \tau), T_L(z, \tau), \frac{\hbar k^2}{2m_c^*}) \quad (11)$$

$$\bar{U}_v = \frac{1}{V} \sum_k \frac{\hbar k^2}{2m_v^*} F(E_{fv}(z, \tau), T_L(z, \tau), \frac{\hbar k^2}{2m_v^*}) \quad (12)$$

The total carrier density and total energy density need to be self consistently calculated in each time step. We can calculate the quasi-Fermi level and instantaneous temperature of the electrons in conduction band based on self consistently theory.

$$\begin{cases} N(z, \tau) = \frac{1}{V} \sum_k F(E_{fc}(z, \tau), T_c(z, \tau), \frac{\hbar k^2}{2m_c^*}) \\ U_c(z, \tau) = \frac{1}{V} \sum_k \frac{\hbar k^2}{2m_c^*} F(E_{fc}(z, \tau), T_c(z, \tau), \frac{\hbar k^2}{2m_c^*}) \end{cases} \quad (13)$$

Similarly, we can also obtain the instantaneous Fermi levels and temperatures in the valence band.

$$\begin{cases} N(z, \tau) = \frac{2}{V} \sum_k F(E_{fv}(z, \tau), T_v(z, \tau), \frac{\hbar k^2}{2m_v^*}) \\ U_v(z, \tau) = \frac{2}{V} \sum_k \frac{\hbar k^2}{2m_v^*} F(E_{fv}(z, \tau), T_v(z, \tau), \frac{\hbar k^2}{2m_v^*}) \end{cases} \quad (14)$$

It should be noted that, the factor of 2 on the right hand of Eq.(14) is observed, because we consider two sub-bands in valence band including heavy hole band and light hole band.

Using Eqs(1-14), we can numerically simulate the dynamics characterization in SOA active region and the signal propagation.

## 2.2 Theoretical model for filtering

OBFs and DIs are typical filters for all-optical signal processing, especially in ultrahigh speed operation scheme. The transmission function of the BPF and the DI can be described as the following two expressions.

$$\begin{cases} F_1(\omega) = \frac{1}{2} [\exp(i\phi) + \exp(i2\pi\tau\omega)] \\ F_2(\omega) = \exp[-2 \ln 2 \cdot (\frac{\omega - \omega_f}{B_0})^2] \end{cases} \quad (15)$$

where  $F_1$  and  $F_2$  are the transmission function of DI and band-pass filters, respectively.  $\phi$  is the phase difference between two arms of the DI,  $\tau$  is the time delay of two arms of the DI.  $\omega$  is the central angle frequency of the BPF,  $B_0$  is 3 dB bandwidth of the BPF. The optical field after SOA can be described as:

$$E_{out}(t) = \sqrt{P_{out}} \exp[i(\omega_0 t + \Phi_{NL}(t))] \quad (16)$$

Based on Fast Fourier Transformer (FFT), the optical spectrum of the output signal after the SOA can be obtained as

$$E_{out}(\omega) = FFT[E_{out}(t)] \quad (17)$$

After optical filtering process, the optical spectrum of the output signals after the two cascaded filters can be described as:

$$E_{opt}(\omega) = E_o(\omega) \cdot F_1(\omega) \cdot F_2(\omega) \quad (18)$$

Then, based on inverse Fast Fourier Transformer (iFFT), the output signal waveform in time domain can be calculated out.

$$P_{opt}(t) = |F^{-1}[E_{opt}(\omega)]|^2 \quad (19)$$

It should be noted that sometimes we should exploit more filters to optimize the output performance, but, the analytical process is identical, adding the transmission function of the new filter in Eq. 17 can get the correct output results.

### 2.3 Applications in all-optical signal processing

For some applications, the configuration and mechanism are fixed and known to us, we can analyze the output performance based on above theoretical model. The analytical process based on the above SOA model and filter model can be illustrated as the following flow diagram.

As shown in Fig.2, based on above SOA theoretical model, we can get output signal waveforms in time domain from SOA and phase variation information is also included in the output signal field. Using FFT tool, we can calculate out the signal spectra. Combing with the filter model iFFT tool, we can simulate out the output signal field. We can optimize the SOA parameters or filter parameters to improve the output performance. This process can be used to optimize the SOA structure and filter shape for special applications.

On the other hand, we can also use the above theoretical model to explore some novel schemes for special signal processing functions. The analytical process can be illustrated as following flow diagram. As shown in Fig.3, for special signal processing functions, input signal and output signal are fixed and known to us, their spectra can be calculated out based on FFT tool, so the transmission functions of the potential schemes can be determined by input spectra and output spectra. Usually, the spectrum transformation process of the SOA is fixed and can be determined by the above SOA model. Using some iteration algorithms, the filtering process and related filters can be optimized.

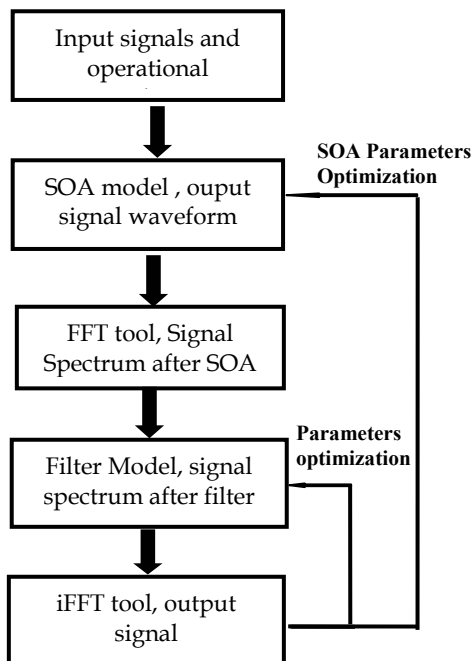


Fig. 2. Analytical process for all-optical signal processing schemes with fixed configurations

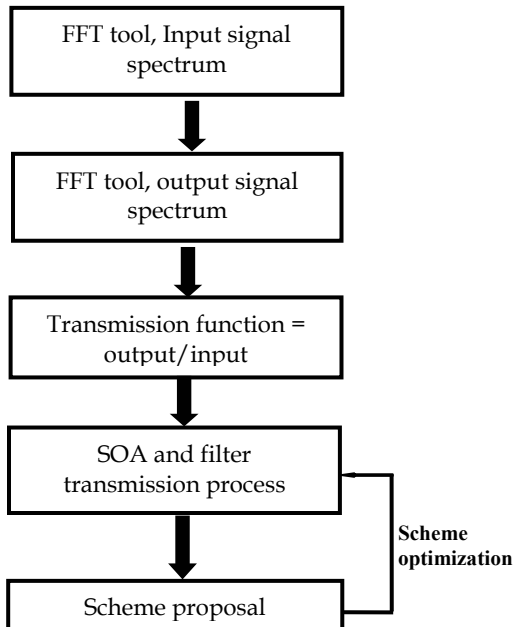


Fig. 3. Analytical process diagram for exploring novel schemes

### 3. All-optical wavelength conversion with SOAs and filters

All-optical wavelength conversion can be regarded as the most important signal processing function because it is the basis of other signal processing functions. In this section, inverted and non-inverted wavelength conversion at 40Gb/s based on different filter detuning were investigated firstly (Dong et al., 2008), then, experimental results on 80Gb/s wavelength conversion and related filtering optimization process are discussed (Huang et al., 2009).

#### 3.1 Bi-polarity wavelength conversion for RZ format at 40Gb/s

Fig. 4 shows the schematic diagram of both inverted and non-inverted wavelength conversion (Dong et al., 2008). A CW probe signal and a data signal with RZ format are launched into an SOA. The following OBF has some detuning to the probe signal with the central wavelength  $\lambda_c + \Delta\lambda_{\text{det}}$ , where  $\Delta\lambda_{\text{det}}$  is the detuning value from probe wavelength at  $\lambda_c$ . The input 40Gb/s RZ signal will induce transient nonlinear phase shifts and intensity modulation to the probe signal via cross phase modulation (XPM) and cross gain modulation (XGM) in the SOA. The nonlinear phase shifts will result in a chirped converted signal with the broadened spectrum. The leading edges of the converted probe light are red-shifted, whereas the trailing edges are blue-shifted. Whether the output converted signal is inverted or non-inverted depends on the detuning value.

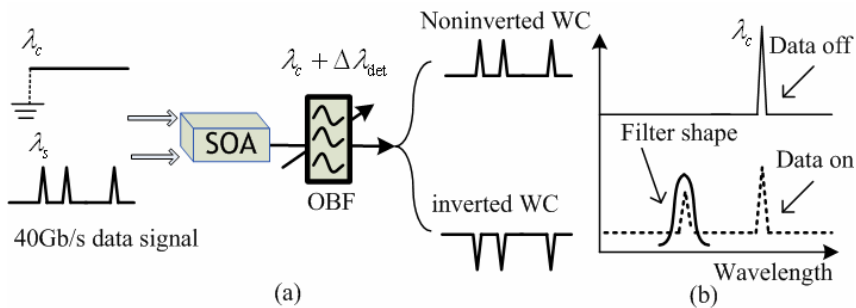


Fig. 4. (a) Operation principle of the bi-polarity wavelength conversion, (b) variation of probe spectrum in the non-inverted wavelength conversion

On the one hand, the wavelength shift of the chirped probe occurs only in the leading/trailing edges of input RZ signals. When the data signal is mark, the probe spectrum will be broadened with sideband energy. If the OBF is detuned far away from the probe wavelength so as to select the sideband energy at  $\lambda_c + \Delta\lambda_{\text{det}}$ , the OBF output will be mark. When the data signal is space, there is no instantaneous frequency shift, and then the OBF output is space, as shown in Fig. 4(b). Therefore, the converted signal will keep in-phase to the input RZ signal. That is non-inverted wavelength conversion.

On the other hand, the XGM will result in the inverted wavelength conversion with relatively slow recovery without the OBF detuning. However, the amplitude recovery can be accelerated and the pattern effects can be eliminated if the OBF is slightly blue shifted. The reason can be explained in Fig. 5. The dotted and dashed lines are the SOA gain and chirp, respectively. When the pulse starts at point A, the SOA carrier depletes and the gain reaches the pit at point B. In time slot from A to B, the probe experiences red chirp and the blue shifted OBF attenuates the probe power. After the pulse duration stops, the gain starts

to recover slowly. Assume that the probe signal gets its maximum blue chirp at point C. After point C, the chirp decreases toward zero, then the blue shifted OBF decreases the transmittance. But the gain recovery is going on. Therefore, the blue shifted OBF can balance the power of blue chirped component and the probe power during gain recovery. As a result, the net power at the OBF output is approximately constant (see time slot from C to D). If the SOA and the OBF are treated as a whole system, the amplitude recovery of the system is much faster than the SOA gain. The fast amplitude recovery technique is also suitable for NRZ format. The detail explanation can be found in reference (Liu et al., 2006).

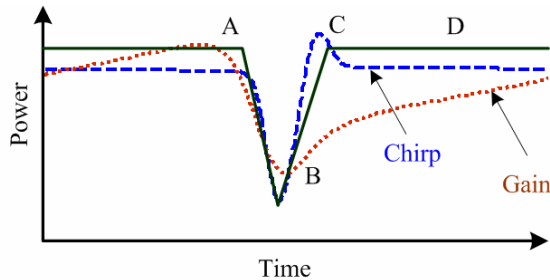


Fig. 5. Principle of accelerating the amplitude recovery.

The experimental setup for bi-polarity wavelength conversion is shown in Fig. 6. Tunable laser diode (LD1) generates a CW probe light at 1557.32nm with the power of 0dBm. Tunable LD2 generates another light source at 1563.5nm, which is modulated by two LiNbO<sub>3</sub> Modulators at 40Gb/s to form a 2<sup>31</sup>-1 RZ pseudo random binary sequence (PRBS) signal, then an erbium-doped fiber amplifier (EDFA) and an attenuator (ATT) are used to fix the RZ output average power at -1.8dBm. The 40Gb/s RZ signal with 8ps-wide pulses is combined with the probe light, and launched into the SOA. The SOA (Kamelian NL-SOA) is biased at 200mA, and its 90%~10% recovery time, defined as the time needed for the gain compression to recover from 90% to 10% of the initial compression, is about 60ps, which is longer than one bit period. The small signal gain@1550nm is 22dB. A tunable OBF1 with bandwidth of 0.32nm follows the SOA. The OBF1 has somewhat detuning to the probe signal to obtain high speed wavelength conversion. Another EDFA and an OBF with 1nm

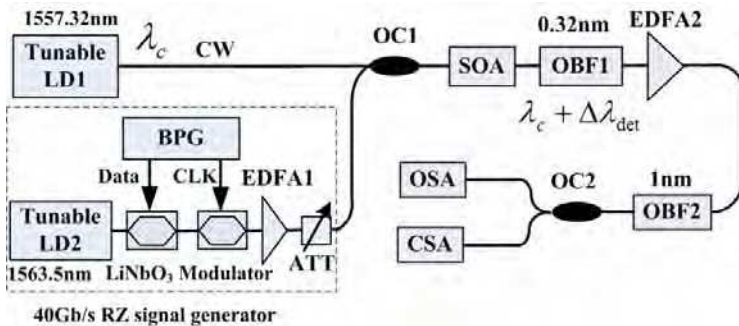


Fig. 6. Experimental setup for bi-polarity wavelength converters at 40Gb/s. BPG: bit pattern generator; ATT: attenuator; OC: optical coupler; OSA: optical spectrum analyzer; CSA: communication signal analyzer.

bandwidth are used to amplify the converted signal power and eliminate the crosstalk. Finally, the optical spectrum analyzer (OSA) and communication signal analyzer (CSA) are used to observe the optical spectrum and waveform of the converted signal.

Fig. 7 shows the experimental results of both inverted and non-inverted wavelength conversion. The left column is the captured waveforms whose time scale is 52ps/div, and the right column is the corresponding eye diagrams whose time scale is 20ps/div. Fig. 7(i) shows the waveform of input 40Gb/s RZ signal. When the OBF1 detuning is -0.3nm (blue shifted) and +0.4nm (red shifted) respectively, the non-inverted wavelength conversion is observed in Fig. 7(ii) and (iv). Good eye diagram is shown in Fig. 7(ii) while some pattern effects occur in Fig. 7(iv). We can see the consecutive marks ①, ②, ③ show a decreasing amplitude. When the OBF1 is slightly blue shifted by 0.1nm, the output waveform becomes inverted and no pattern effects occur, shown in Fig. 7(iii). When the OBF1 has the same central wavelength to the probe carrier, the output waveform has very serious pattern effects, shown in Fig. 7(v). Therefore a slightly blue shifted OBF can accelerate the amplitude recovery in the inverted wavelength conversion.

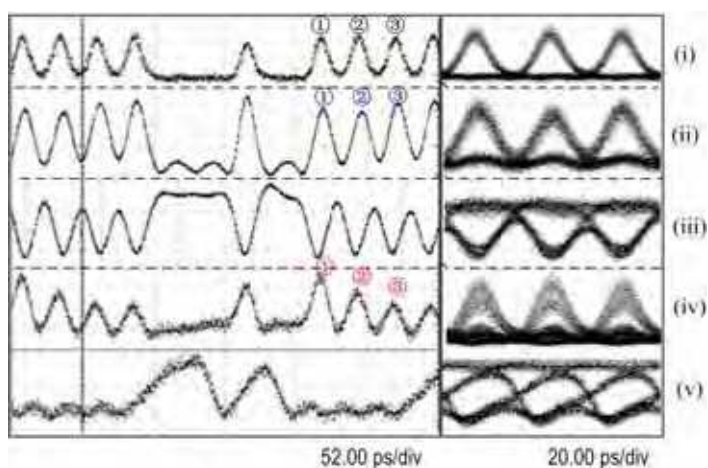


Fig. 7. Waveforms of converted signal with different detuning, (i) the input RZ waveform, (ii)-(v) are the output waveforms of converted signal when the OBF1 detuning is -0.3nm, -0.1nm, +0.4nm, and 0nm, respectively. The left column and right column are the captured waveforms and eye diagrams.

The experimental results can be explained from the spectrum. Fig. 8 shows the spectra of converted signal when the OBF1 is detuned. The probe spectra before and after the SOA are shown in Fig. 8(a). At the SOA output, the probe spectrum is broadened asymmetrically due to the XPM. The output spectra of converted signals are shown in Fig. 8(b)-(e) corresponding to the OBF1 detuning -0.3nm, -0.1nm, +0.4nm, and 0nm, respectively. In Fig. 8(b), the blue sideband of converted signal becomes dominant with the assistance of the blue shifted OBF1, therefore good eye diagram could be observed. While in Fig. 8(d), the OBF1 cannot suppress the probe carrier. The crosstalk between red sideband peak and probe carrier will result in the pattern effects in time domain. In Fig. 8(b) and (d), the OBF1 detuning is different for achieving the best non-inverted wavelength conversion because of the asymmetric probe spectrum at the SOA output. Besides, the negative slope of OBF1 is

larger than the positive slope, so the blue shifted OBF is easy to suppress the probe carrier, but red shifted OBF is not. In Fig. 8(c), the probe carrier keeps dominant, so the output waveform becomes inverted.

The non-inverted wavelength conversion with blue shifted OBF shows better performance than red shifted OBF. This can be explained with the chirp characteristics. Fig. 9(a) shows the input RZ signal with four consecutive bits "1", and Fig. 9(b) shows the probe phase variation at the SOA output. One can see that the phase increases fast in the leading edge, which corresponds to carrier depletion. However the phase decreases slowly in the trailing edge, which results from the carrier recovery. Fig. 9(c) shows the probe chirp, which is the first order derivative of the phase variation by contrariety. With consecutive "1" pulses injection, the carrier depletion decreases, then the red peak chirp decreases as well. This leads to the decreasing amplitude of the converted pluses by means of the red OBF transfer function (see ①, ②, ③ of the red OBF), and the converted pulses show serious pattern effects. On the other hand, one notices that the blue peak chirp increases very slowly, and remains constant approximately. This results from the similar carrier recovery under consecutive "1" pulses injection. By means of the blue OBF transfer function, the amplitude of converted pulses remains constant (see ①, ②, ③ of the blue OBF). Therefore, the non-inverted wavelength conversion performance is better with blue shifted OBF than with red shifted OBF.

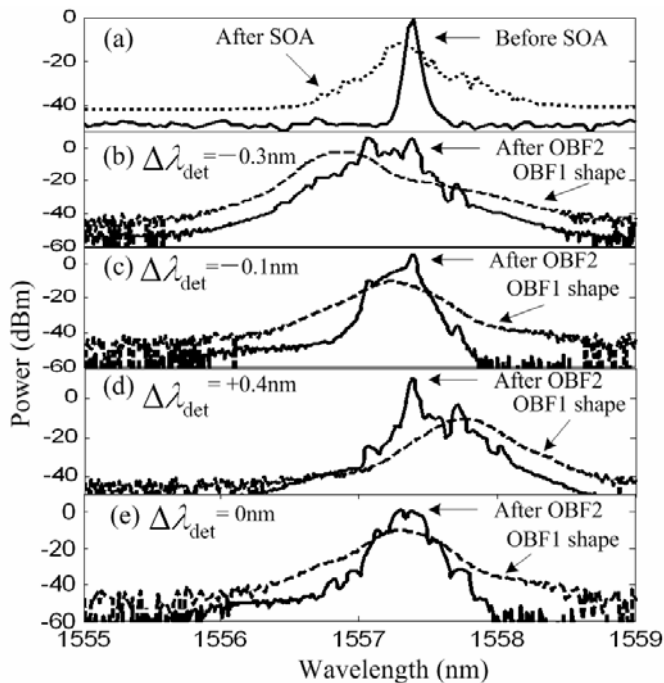


Fig. 8. Spectra of converted signal with different detuning, (a) the probe spectrum before and after SOA, (b)-(e) are the output spectra of converted signal when the OBF1 detuning is -0.3nm, -0.1nm, +0.4nm, and 0nm, respectively.

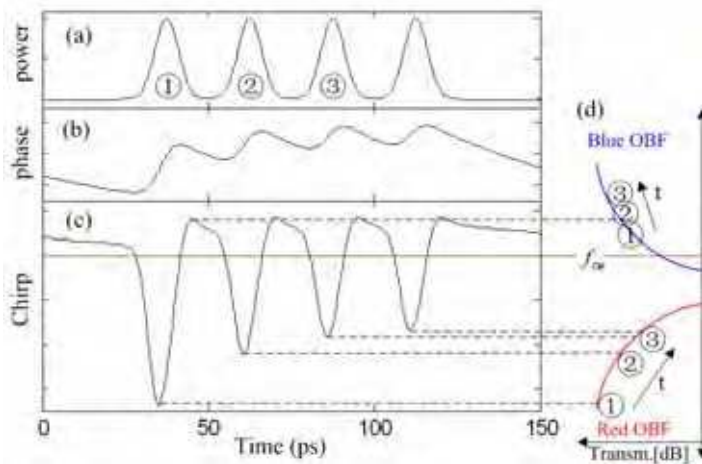


Fig. 9. Comparison of blue shifted OBF and red shifted OBF by frequency-amplitude conversion at the OBF slopes, (a) consecutive “1” pulses, (b) phase evolution, (c) chirp evolution, (d) frequency-amplitude conversion.

The wavelength tunability is further investigated in our experiment. For ease of discussion, we only adjust the wavelength of tunable LD2. We investigate the output extinction ratio (ER) under the optimal OBF1 detuning, as shown in Fig. 10. The output ER fluctuates around 7dB in the whole C-band (1528-1563nm), except the near region of RZ wavelength. The inset of Fig. 10 shows the SOA amplified spontaneous emission (ASE) spectrum, which reveals that the SOA gain is low at the shorter wavelength. Therefore the ER decreases at shorter wavelength. Our experiment scheme cannot complete the wavelength conversion of the same wavelength since the OBF cannot separate the probe and signal channels at the same wavelength.

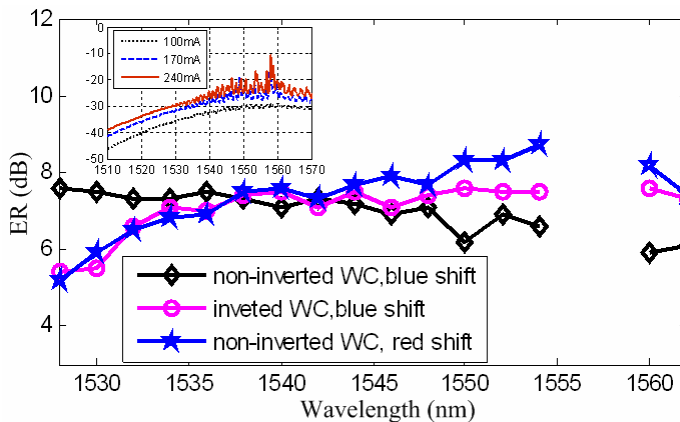


Fig. 10. Output ER as a function of the input signal wavelength when the OBF1 detuning is -0.3nm, -0.1nm, and +0.4nm, respectively. The inset is the SOA ASE spectra at different bias currents.

From Fig. 10, we can see that the output ER is not very high in the three kinds of wavelength converters. The reasons resulting in low ER are quite different between inverted wavelength conversion and non-inverted wavelength conversion. For non-inverted wavelength conversion, the OBF1 does not have a sharp slope, which could not separate the sideband signal from the probe spectrum completely, as shown in Fig. 8(b) and (d). Therefore, the crosstalk between the sideband signal and the probe carrier will degrade the output ER. For inverted wavelength conversion, we need ultrashort pulse injection to enhance the T-XPM effect and to generate large chirp of the probe signal. However, the 8ps-wide input pulses are not narrow enough to obtain inverted wavelength conversion with large ER. We believe the output ER could be improved if the OBF slope is optimized and the input RZ pulses are compressed as narrow as possible.

### 3.2 80Gb/s wavelength conversion with SOA and cascaded filters

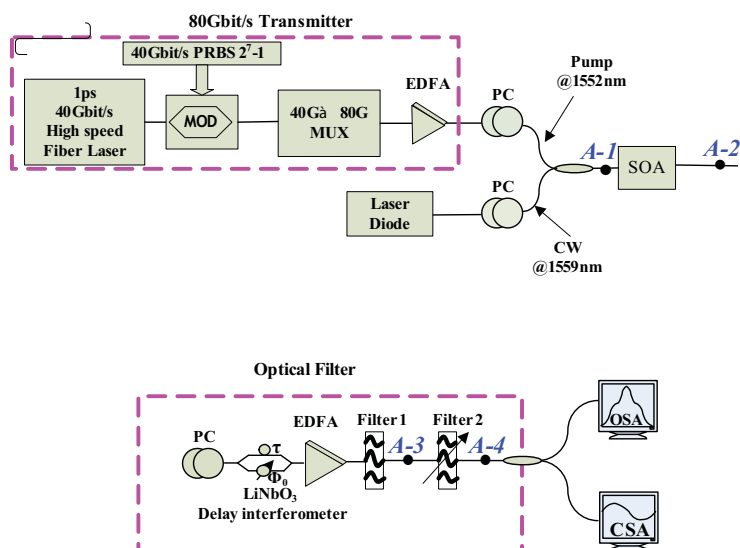


Fig. 11. Experimental setup for 80Gb/s wavelength conversion with SOA and cascaded filters: PC: Polarization controller, EDFA: Erbium-doped fiber amplifier, OSA: optical spectrum analyzer; CSA: communication signal analyzer.

The experimental setup is shown in Fig.11 (Huang et al., 2009). A 40GHz 1.0-ps wide (FWHM) optical pulse is modulated by an external amplitude modulator (MOD) at 40Gbit/s to generate a 2<sup>7</sup>-1 RZ-PRBS signal. This data stream is then optical time multiplexed (MUX) to 80Gbit/s. After amplification, the average optical power of the 80Gbit/s data stream is 4.8mW and the continuous wave (CW) probe signal is 3mW. After the polarization controller, the 80Gbit/s signal is combined with the CW probe and fed into an SOA via 3 dB coupler. As shown in Fig.12, the cascaded filtering model is consisted of a 3.125 ps delay LiNbO<sub>3</sub>-DI, an optical band-pass filter 1 with bandwidth of 3 nm and the tunable optical band-pass filter 2 with bandwidth of 1 nm which is detuned 1.2 nm to the blue side of the probe carrier wavelength. An inverted 80Gbit/s signal can be obtain at the output of the SOA. The converted signal is subsequently injected into the LiNbO<sub>3</sub> DI, where

the inverted signal is converted into a non-inverted signal. At the output of the tunable optical band pass filter 2, the non-inverted probe signal is monitored by using an optical sampling scope; the optical spectrum is analyzed by using an optical spectrum analyzer (OSA) with a resolution of 0.050 nm, simultaneously. In our experimental setup, the SOA is biased at 250mA.

It should be noted that, the sampling frequency of the OSA used in our experiment is 40GHz, while the data stream is modulated at 80 Gb/s. Thus the short pulse monitored by the OSA is broadened. However, we are still able to distinguish the eye opening and ER of the output waveform which are shown in Fig.13 (b), (c), (d).

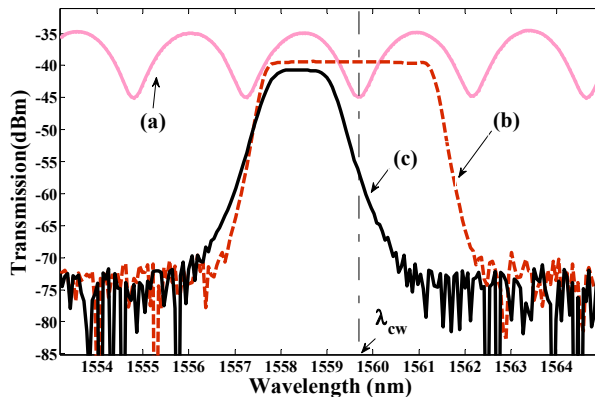


Fig. 12. Transmission spectra the DI (a-1), the band pass filter 1(a-2), the band pass filter2 (a-3).

The operation principle for optical spectrum filtering base on SOA is described as follows. An ultra-fast pulse-stream is combined with a CW probe light and launched into the SOA. The pump signal will induce nonlinear phase shift to the probe signal via T-XPM in the SOA, As a result, the spectrum of the probe signal is broadened. To obtain the high output quality, we optimize the spectrum filter using the LiNbO<sub>3</sub> DI and band-pass filters. As seen curve (a) in Fig.12, the “notch” characteristic of LiNbO<sub>3</sub> DI is clearly visible. An important feature to be noted is that for the non-inverted output, the wavelength of the notch is set to be the center wavelength of the converted probe signal, ensuring a high attenuation of DC component corresponding to the “1” level in the inverted signal and a larger transmittance of the “0” level. On the other hand, the LiNbO<sub>3</sub> DI modifies the spectrum of the output probe of SOA. The central wavelength of the filter 1 is fixed at carrier wavelength of the probe signal. Thus, the pump signal is suppressed and the power ratio of the probe and pump signal is about 30dB (seen in Fig.13 (A-3)). Another low-noise EDFA 2 is applied to amplify the output signal. Then, we use the filter 2 to extract out the component at the central wavelength  $\lambda_c + \Delta\lambda$ , where  $\lambda_c$  is the central wavelength of the probe signal,  $\Delta\lambda$  is the detuning value from  $\lambda_c$ . In this experiment, probe wavelength  $\lambda_c$  is 1559.89nm, and the wavelength detuning  $\Delta\lambda$  is -1.2nm.

Fig.13 (a) depicts the optical spectrum measurement at the different position of the experimental setup. Fig.13 (b-d) shows the measured eye diagrams. Fig.13 (b) is the input pump signal at 1541nm, Fig.13(c) shows the eye diagram of the output signal after the OBF1, and Fig.13 (d) depicts output signal after OBF2. They all show good eye-opening

performance, the ER of input pump signal is 13.529dB, while the ER of output signal after the BPF 1 is only 3.291dB, and the ER of output signal after the OBF 2 is as high as 20.00dB.

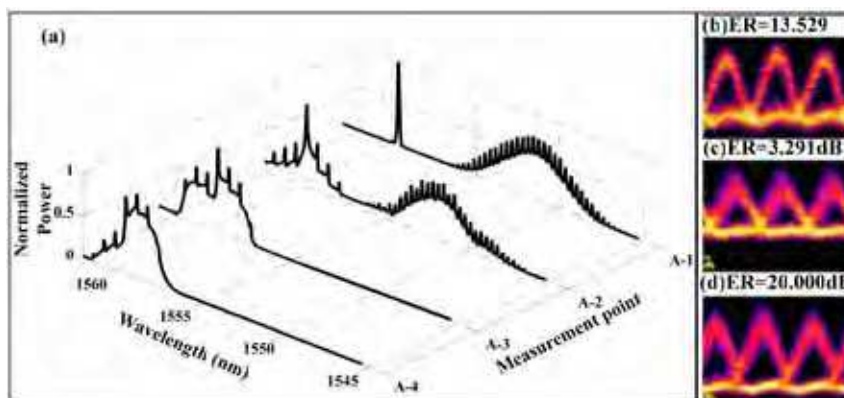


Fig. 13. Experimental results for 80Gb/s wavelength conversion (a) the optical spectrum measurement at different position corresponding to Fig.11; Eye diagram for (b) input pump signal at 1552nm, (c) output probe signal after OBF 1, (d) output probe signal after OBF 2

For wavelength conversion with SOAs, XGM, XPM, FWM and Transient XPM effects can all be exploited. However, for different operation conditions, one main effect dominates over other effects which maybe improve or degrade the output signal performance. Therefore, optimization of SOA parameters, filtering parameters and operational conditions is very important to get better output performance, and this optimization process can be achieved based on theoretical model presented in section 2.

#### 4. All-Optical logic operation with SOAs and filters

In this section, we will focus on experimental study for all-optical logic operation based on SOAs and filters. Three schemes for all-optical logic operation were introduced. Firstly, All-optical logic AND gate at 40Gb/s based on XGM in cascaded SOAs was presented (Xu et al., 2007), and operation condition and output performance were analyzed. Secondly, based on single SOA and different filtering processing, five different logic gates were demonstrated (Dong(b) et al., 2007; Dong et al., 2008; Wang et al., 2007), different nonlinear effects such as XGM, FWM, Transient XPM are exploited in different logic gates respectively. Thirdly, a flexible scheme for all-optical minterms generation was proposed and demonstrated (Xu(a) et al., 2008; Xu(b) et al., 2008). Based on DI and XGM of SOAs, all-optical minterms for two input signals and three input signals were realized respectively.

##### 4.1 All-optical logic AND gate based on cascaded SOAs

It is known that the logic function of inverted wavelength conversion can be written as  $\bar{A} \cdot B$  given that data signal A and B are used as pump and probe light respectively. Particularly, it degenerates into a NOT gate when a continuous-wave (CW) serves as the probe light. Therefore, AND gate can be realized by cascading two sets of SOA and filter and configuring the first one as a NOT gate, i.e.  $A \cdot B = \overline{(\bar{A})} \cdot B$  (Zhang et al., 2004).

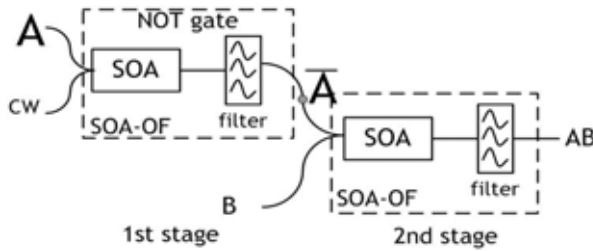


Fig. 14. Schematic diagram for all-optical logic AND gate with cascaded SOAs

As shown in Fig. 14 (Xu et al., 2007), a continuous wave (CW) beam is used as an intermediate wavelength connecting two stages. As probe light at the first stage, it is converted into the negated signal of data A at the output of first stage and serves as pump light at the second stage. Note that the optical filter mentioned above particularly refers to the one who effectively reshapes the spectrum of the modulated probe light. If pump wavelength can not be blocked by such OF, additional optical filter should be used to set the pump and probe wavelength apart.

The experimental setup for the ultrafast AND gate is shown in Fig. 15. In this experiment, three wavelengths generated by LD1, LD2, LD3 are 1560nm( $\lambda_1$ ), 1549.32nm( $\lambda_2$ ) and 1555.75nm( $\lambda_c$ ) respectively.  $\lambda_1, \lambda_2$  are modulated by Transmitter simultaneously with 2<sup>7</sup>-1 pseudo-random binary sequence (PRBS) RZ data streams at 40Gb/s. The duty cycle of these RZ pulses is 33%. Two wavelengths are separated by a demultiplexer (DMUX) and the optical delay line (ODL) is used to synchronize the input data sequences at the second stage. Thus, two quasi-independent data signals at  $\lambda_1$  and  $\lambda_2$  are obtained at the input of SOAs.  $\lambda_c$  is used as intermediate wavelength. The time delay of DI is 25ps which equals to the single bit period of 40Gb/s data rate. The optical BPF following the DI is used to extract the probe light. The filtered probe light is amplified before coupled into the second SOA. The 3dB bandwidth of the Tunable BPF is 0.32nm. The average optical power measured at the input of SOA1 are 7.93dBm( $\lambda_1$ ) and 5.92dBm( $\lambda_2$ ), while 3.10dBm( $\lambda_2$ ) and -17.92dBm ( $\lambda_c$ ) at the

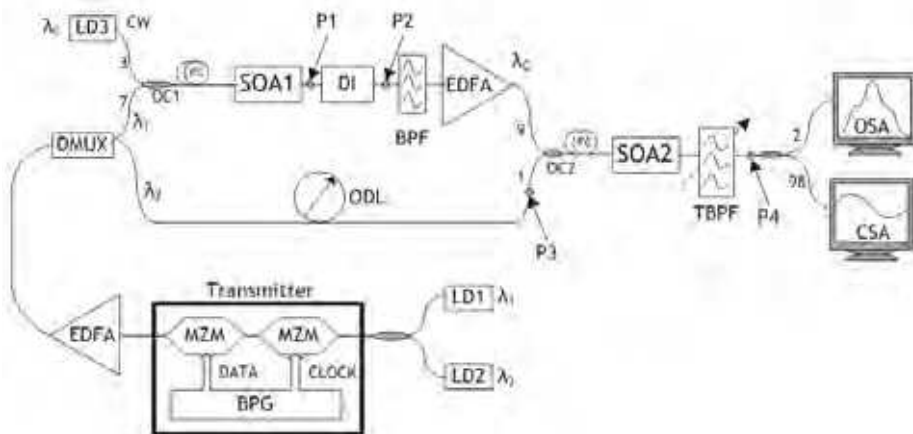


Fig. 15. Experimental setup for all-optical logic AND gate at 40Gb/s with cascaded SOAs

input of SOA2. AND logic results can be achieved through properly tuning the notches of DI and the center wavelength of tunable BPF. In our experiment, the transmission spectrum of the DI can be tuned by adjusting the operational temperature of DI.

Fig. 16 shows the AND logic results (R6) of data signal R7 and R5. R3 is the negated signal of R7, which is NRZ format due to the equivalency between the time delay of DI and the single bit period. The ER of measure AND results is 8.8dB. The bottom trace shows the eye diagram of derived AND results which display open and clear eyes. The QF of the measured eyes is 6.3.

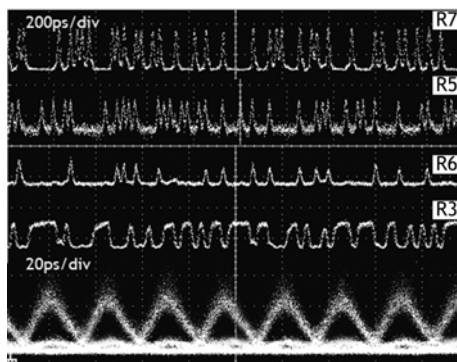


Fig. 16. Output experimental results for all-optical logic AND gate

It should be noted that the SOA1 is a slow recovery bulk material SOA which carrier recovery time is about 500ps. In this SOA, XPM effect is very strong which dominates the output performance. The DI is used to demodulate the phase modulation process, the time delay equals to the bit period, therefore, RZ input signal is wavelength converted to a NRZ signal. The SOA2 is a fast recovery ultrafast SOA which carrier recovery time is about 60ps. The following narrow bandpass filter is detuning from the signal B, the detuning process can be optimized to get the best output performance according to the theoretical model in section 2 and analysis of accelerating mechanism in section 3. On the other hand, the most important factor for good AND results is the extinction ratio of the converted signal from stage 1. If we want to improve the output performance or increase the operation speed, the parameters of SOAs and filtering processes should be optimized.

#### 4.2 Configurable all-optical logic gates based on single SOA and tunable filter

In this subsection, we propose and experimentally demonstrate reconfigurable all-optical logic gates based on various nonlinearities in single SOA (Dong(b) et al., 2007; Dong et al., 2008). The operation principle of the configurable logic gates is described in Fig. 17. Data  $A$  and  $B$  are the data signals to be processed, whose wavelengths are  $\lambda_A$  and  $\lambda_B$ , respectively. The probe signal is a CW at wavelength  $\lambda_C$ , which will be gain- and phase-modulated by the data signals through the SOA. Thus the output optical spectrum of the probe signal will be broadened. Different logic gates can be realized at different OBF setting.

When both data signals are presented in the SOA, the conjugated light is generated due to FWM effect. The converted signal can be optically filtered out to implement AND logic. When either data  $A$  or  $B$ , or both are presented, the probe signal is gain-modulated with polarity-inverted output, which is logic NOR gate. Whereas, the slow gain recovery of SOA

## Thank You for previewing this eBook

You can read the full version of this eBook in different formats:

- HTML (Free /Available to everyone)
- PDF / TXT (Available to V.I.P. members. Free Standard members can access up to 5 PDF/TXT eBooks per month each month)
- Epub & Mobipocket (Exclusive to V.I.P. members)

To download this full book, simply select the format you desire below

